Directly-Grown Germanium Nanowires from Stainless Steel: High-performing Anodes for Li-Ion Batteries

David McNulty[1], Subhajit Biswas[1,2], Shane Garvey[1], Colm O'Dwyer[1] and Justin D. Holmes[1,2]*

[1]School of Chemistry and Tyndall National Institute, University College Cork, T12 YN60, Cork, Ireland. [2]AMBER Centre, Environmental Research Institute, Cork, T23 XE10, Ireland

*To whom correspondence should be addressed: Tel: +353 (0)21 4903608; Fax: +353 (0)21 4274097; E-mail: s.biswas@ucc.ie (SB)

Abstract

Germanium (Ge) nanowires were fabricated directly on stainless-steel current collectors for Li-ion battery, without any additional catalytic seeds. Substrates of stainless-steel is an unconventional material for the direct growth of nanowires for battery applications. Stainless steel substrates were activated for nanowire growth by annealing them in air at a temperature of 450 °C to form a catalytic iron oxide surface layer. Large yields of Ge nanowire were obtained from oxidised stainless steel via a liquid-injection chemical vapour deposition process, with diphenylgermane (DPG) as Ge precursor. Fabricated Ge nanowires have uniform morphology and are single crystalline. The capacity retention from a nanowire anode tested at 0.2 C is very stable, highlighted by a reversible capacity of ~ 1014 and 894 mAh/g after the 50th and 250th cycles, respectively. The large specific capacity values are one of the highest achieved for binder-free Ge nanomaterials based anode materials. The high specific capacity values, good capacity retention and voltage stability observed resulted from the excellent adhesion of the nanowires to the stainless-steel current collectors, ensuring good electrical

contact and electrical conductivity. Achieving such electrochemical performance from Ge nanowires grown via a significantly simplified direct growth process on a functional conductive substrate demonstrates the potential of directly grown Ge nanowires as a high performing anode material for Li-ion batteries.

Keywords: Germanium, Nanowire, Stainless Steel, vapour-solid-solid, Li-ion battery

Introduction

In recent years, there has been a tremendous research effort to identify a suitable replacement for graphite as an anode material in Li-ion batteries. The ultimate aim is to increase the specific energy of commercial cells to achieve ever-growing energy storage demands..[1–5] Group IV semiconductors such as Si and Ge have great potential as anode materials in Li-ion battery as they have significantly higher theoretical capacities than graphite (theoretical capacity of 1620 mAh/g for Ge and 3579 mAh/g for Si).[6–8] Si has garnered more attention than Ge as Li-ion battery anode material due to its increased theoretical capacity. However, Ge is kinetically superior and have higher electrical conductivity, ~100 times higher than that of Si. Additionally, Li-ions diffuses faster in Ge than in Si at room temperature.[9,10] But the drawback in using Ge (or Si) as anode in Li-ion battery is the significant volume expansion upon lithiation. This leads to pulverisation and consequently the reduced cycle life and capacity retention for Li-ion battery. Various Ge nanostructures morphologies, *e.g.* nanoparticles, microflowers, nanosheets and nanotubes[11–14] have been used as anode materials for Li-ion anodes in an attempt to mitigate issues associated with volume expansion. There are also additional benefits of using Ge nanowires as an anode material, including the high interfacial area of the nanowires in direct electrolyte contact, short Li-ion diffusion path lengths and good electrical conductivity along their lengths.

Additional metal catalysts (Au, Sn, Ni, Cu, Pb *etc*.) are usually utilised in a conventional three phase growth process (vapour-liquid-solid or vapour-solid-solid) for the fabrication of diameter controlled nanowires[7,15–20] on current collectors. These additional metals can contribute both positively, *e.g.* Sn and negatively, *e.g.* Au, to the specific capacity of the anode material.[19,21] Recently, Ge (or Si) nanowires were directly grown on current collecting metallic substrates (Cu, Ni *etc*.) for Li-ion battery applications due to the ease of electrode fabrication

with good electrical contact.[20,22,23] For the direct nanowire growth, the metallic substrates (Cu, Ni) used are conventional type C catalyst metal, forming stable germenide compounds during growth, in the vapour-solid-solid (VSS) bottom-up growth of Ge (or Si) nanowires. The growth of Ge nanowires on Cu foils has been reported via the thermal decomposition of metal-organic germane in the solvents with high boiling point.[23] Stainless steel is not only a cost-effective alternative to Cu current collectors but is also stable when heated to high temperatures. Stainless steel have been used previously as current collector for nanowire anodes such as silicon nanowires in Li-ion battery.[24] However, only limited growth of Ge nanowire was previously observed on polished Fe surface using customised metal-organic precursors.[25] For the implementation of Ge nanowires in Li-ion anodes, it would be beneficial to grow high yields of these nanowires on commercially available stainless steel foils (current collectors). Additionally, preparation of a slurry of the active material with a conductive additive and a binder is not required when the nanowires are grown directly onto a stainless-steel current collector.

In this article, we report the growth of Ge nanowires on 316 L stainless steel foils, by inducing an iron oxide catalytic layer on their surfaces, via a vapour-solid-solid (VSS) three-phase growth. The direct growth of nanowire anode material on bulk current collectors not only has the potential to make the electrode fabrication process cost-effective and simple, but can potentially result in improved electrical contact between the anode and the current collector; ultimately contributing towards increased electrical conductivity, shorter Li ion diffusion distances and high specific capacities. Utilising the current collector itself as the nanowire growth promoter and substrate can further establish good mechanical contacts at the collector-electrode interface, thus minimising detachment of the nanowires from the current collector upon volume expansion. The high capacities (~ 900 mAh/g after 250 cycles) and

impressive capacity retention reported here verifies the great possibility of the directly-grown Ge nanowires from stainless steel as Li-ion battery anode materials.

Results & Discussion

To begin with, the novel direct growth of Ge nanostructures on a stainless-steel current collector is explored for use as anode material for Li-ion batteries. Nanowires were grown using a modified bottom-up method we previously reported using Fe_3O_4 nanodots as growth promoters.[26] A liquid-injection CVD approach was utilised for the growth of Ge nanowires, with DPG as Ge precursor on stainless-steel substrates and at a temperature of 440 °C (see Supporting Information for detailed experimental approach). Heating stainless-steel in air, prior to nanowire growth, at 450 °C leads to the formation of a thin (usually < 50 nm) surface oxide, predominantly consist of Fe oxides.[27] Annealing stainless steel at this oxidation temperature (450 °C) usually forms Fe_2O_3 phase on the surface and creates a surface with granular texture with very small particulates. (Figure S1 in the Supporting Information shows scanning electron microscopy (SEM) images and X-ray photoelectron spectroscopy (XPS) spectra of the treated stainless steel showing the formation Fe_2O_3 phase of iron oxide). The moderate nanowire growth temperature of 440 °C ensures sufficient seeding of Ge nanowires from the iron oxide nanoparticles, formed on the stainless steel surface, through a vapour-solid-solid (VSS) mechanism.

Figures 1(a) and (b) depict (SEM) images of Ge nanowires grown from oxidised stainless-steel substrates. The SEM image in Figure 1(a) highlights the formation of long nanowires (> 5 μm), with uniform radial dimensions along their lengths and a mean diameter of 60 (±5.1) nm based on TEM analysis of 100 nanowires. There was also a high coverage of

the stainless-steel substrates with nanowires. SEM image also depicts very little evidence of the formation of spherical particulates due to homogeneous nucleation of Ge. Direct growth of the nanowires from the stainless steel substrate is evident from the side-view SEM image (Figure S1 (d), Supporting Information). Nanowires grown on 'unactivated' stainless steel substrates, *i.e.* that were not heated to a temperature of 450 °C in air, were significantly shorter in length (< 1 μm), as portrayed in Figure 1 (c) and (d), compared to those grown on 'activated' substrates. Significant quantities of spherical aggregates were also formed on "unactivated" substrates as shown in Figures 1 (c) and (d). Furthermore, a large decrease in the relative yield of nanowires was obtained for the "unactivated" substrates compared to the oxidised substrates, 15 μg compared to 144 μg respectively, confirming the significance of the surface iron oxide layer in producing high yields of Ge nanowires from stainless steel foils.

Ge nanowire growth from the stainless steel substrate should follow a sub-eutectic vapour-solid-solid (VSS) growth paradigm, as the nanowire growth temperature (440 ºC) is far below the eutectic temperature (lowest eutectic at ~ 850 ºC) of Fe-Ge. Among the germanide forming metal catalysts with high eutectic temperature, Cu is the most suitable for the direct growth of Ge nanowire from metal foils due to the high solid solubility of Ge in Cu, relatively low eutectic temperature (644 ºC), and the low supersaturation (~ 20 at.%) of Ge in Cu in the sub-eutectic regime. In contrary, a very high supersaturation (70 %) of Ge is needed for $FeGe_2$, predicted phase of stable germenide compound according to the "first phase rule", formation and Ge nanowire growth.[26] In VSS-type growth, with a type-C catalyst, stable germanide compounds are formed via the diffusion and thermal decomposition of the precursor in the metal catalyst. Metallic Fe can transform into $FeGe_2$ at our growth temperature with Ge uptake (via forming a solid solution) from the source.[28] This could be a kinetically slow process due to the high supersaturation required for $FeGe_2$ formation, slow diffusion and low solid

solubility of Ge in Fe.[29] Whereas, a solid state reaction govern $FeGe_2$ formation from Fe_2O_3 and is driven by the incorporation of germanium into the Fe_2O_3 lattice through a substitution mechanism.[26] Experimental observation of vastly high nanowire yield with the oxidised stainless steel substrate compared to the "unactivated" stainless steel (Figure 1) confirms solid state substitution reaction of Fe_2O_3 as kinetically favourable mechanism for germanide formation at our growth temperature. Additionally, the sub-eutectic growth of Ge nanowires from metal oxide seeds typically result in faster growth and the formation of uniform diameter nanowires.[30] Also, the surface iron oxide catalytic seed layer can act as catalyst for the precursor decomposition.[31] This catalytic activity can promote nanowire formation from the organometallic precursors at relatively lower growth temperatures, 440 ºC in our case.

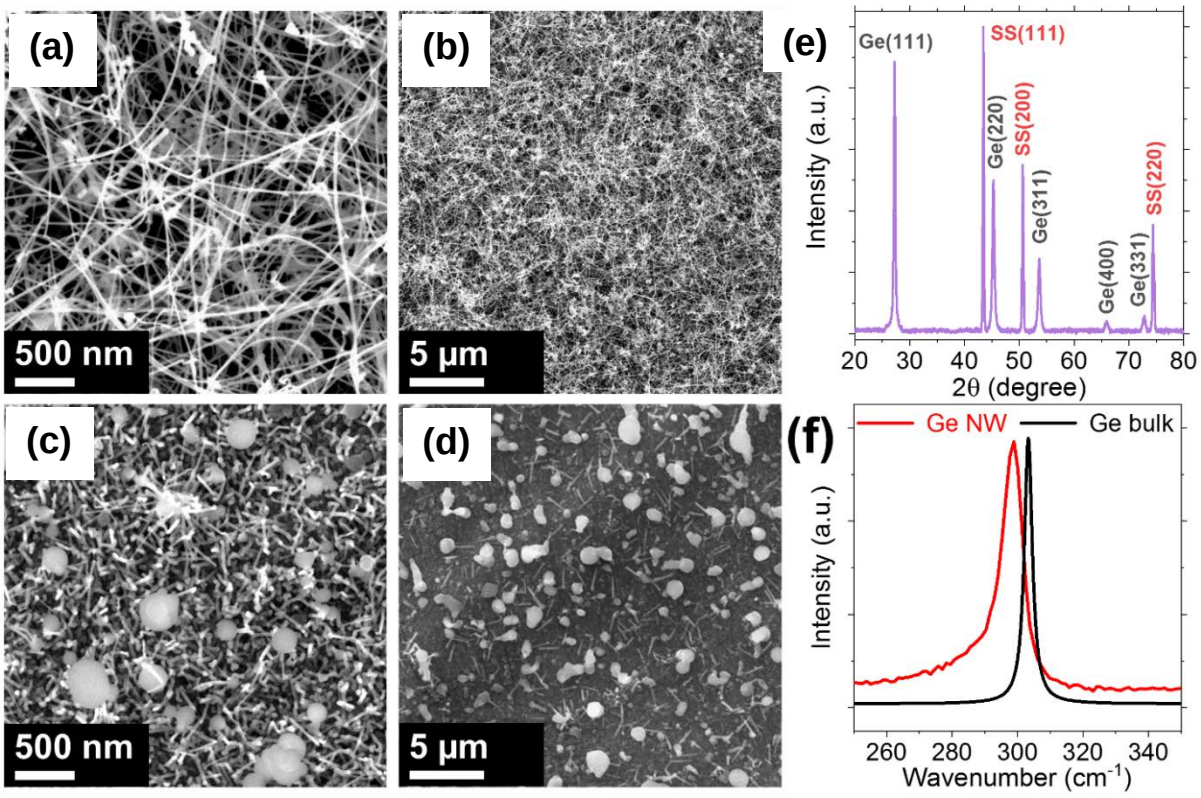

Figure 1. (a) and (b) SEM images of Ge nanowires grown on 'activated' oxidised stainless-steel substrates, taken at different magnifications. (c) XRD pattern confirms the formation of diamond cubic Ge nanowires on oxidised stainless steel. Part (d) and (e) show SEM images of

Ge nanowires grown on ‘unactivated’ (as received) stainless steel substrates taken at different magnifications. (f) Room temperature Raman spectrum of Ge nanowires and bulk Ge.

As bulk tools, X-ray diffraction (XRD) and Raman spectroscopy are efficient in determining the purity of the crystal and phase of the nanowires. The XRD pattern obtained from the Ge nanowires (Figure 1(e)) matches well with the diamond cubic germanium lattice (JCPDS card no. 04-0545). Three XRD peaks at 2θ values of 27.3, 45.3, and 53.5° correspond to the (111), (220), and (311) set of planes for the diamond cubic germanium lattice, whereas the other reflections can be assigned to the 316L stainless-steel substrate.[32,33] The XRD pattern did not show any diffraction peaks corresponding to iron germanide, i.e. tetragonal $FeGe_2$. It is very difficult for a conventional XRD to determine a dilute secondary phase of nanoscale dimension, such as the formation of $FeGe_2$ at the tip of the nanowires. Figure 1(f) shows the Raman spectrum of an as grown Ge nanowire sample grown on a stainless steel substrate. The strong peak around 298.6 cm^{-1} is attributed to the triply degenerated E_{2g} vibration (Ge-Ge mode).[34] The Ge-Ge Raman peak can shift to a lower energy for the nanowires compared to bulk Ge, due to phonon confinement or strain in the nanowires.[34] A red shift of 3 cm^{-1} of the Ge-Ge longitudinal optical (LO) mode was detected for nanowire with the average diameter of 60 nm compared to bulk Ge (Figure 1 (f)).

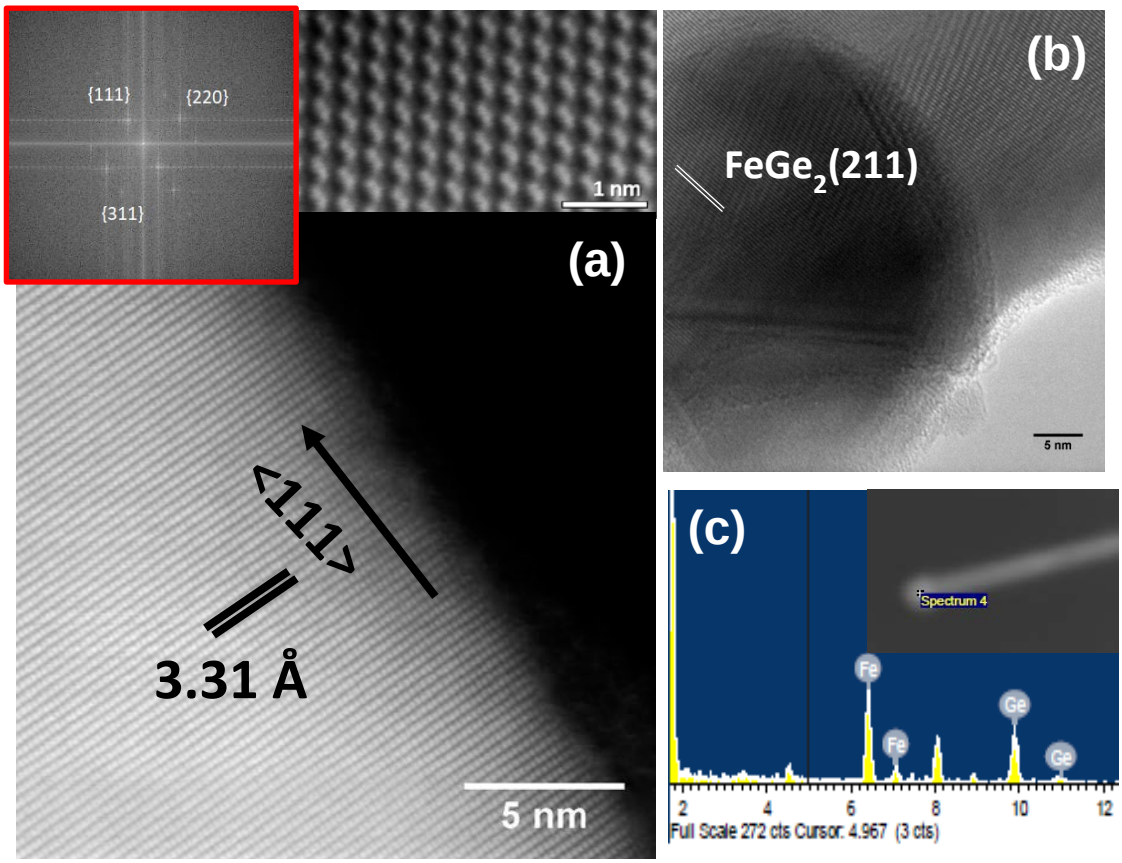

Figure 2. Dark field STEM image in part (a) depicts single crystalline nanowire with <111> growth direction. Right inset in the part (a) shows the dumbbell like configuration with interplanar spacing corresponding to (111) plane of diamond cubic Ge. Left inset shows FFT pattern from the HRTEM. (b) HRTEM image near the catalyst-nanowire junction shows $FeGe_2$ phase at the nanowire tip. (c) EDX spectra recorded from the catalytic of the nanowire confirms $FeGe_2$ composition of the tip (peak ~ 8 keV corresponds to Cu from the TEM grid).

The structural quality of the Ge nanowires was further confirmed by high-resolution TEM (HRTEM) and high-resolution scanning transmission electron microscopy (STEM) imaging (Figure 2). Most of the nanowires synthesised from the stainless-steel substrates depicted no roughness of the surface. These nanowires were highly crystalline with a low amount of crystal defects such as twin boundaries and stacking faults (HRSTEM image in Figure 2(a)). All nanowires possessed a diamond-cubic crystal structure (JCPDS cards #04-0545), confirmed from the HRSTEM and the corresponding Fast Fourier Transform (FFT) pattern analysis. The preferred growth direction of nanowires is assigned as <111> (from FFT

analysis in the right inset of Figure 2(a)). Interplanar spacing (*d*), determined from the HRTEM analysis, in nanowires is slightly larger (*d*= 0.33 nm) than the *d* value reported for bulk diamond Ge crystals (0.326 nm from the JCPDS 04–0545). HRSTEM and corresponding FFT are recorded with <110> zone axis alignment. The HRSTEM image from the centre part of a Ge nanowire (the right inset of Figure 2(a)) shows a typical Ge dumbbell arrangement. The presence of tetragonal $FeGe_2$ as the final phase of the growth catalyst was confirmed from the HRTEM image (Figure 2 (b)). The interplanar spacing of 0.23 nm matches well with the bulk lattice spacing of (211) plane of tetragonal $FeGe_2$ (*d*= 0.232 nm from JCPDS cards #75-0033). Ge nanowire with a $FeGe_2$ alloy tip confirms the likelihood of a vapour-solid-solid (VSS) growth mechanism in the formation of the nanowires. The presence of catalytic spherical particles at the tip of the nanowire provides further evidence of catalytic growth of nanowires, as shown in the low resolution high angle annular dark-field (HAADF) STEM analysis (Figure S2 in Supporting Information). Energy dispersive X-ray (EDX) point-analysis in dark field STEM were also performed on the spherical nanoparticle tips to confirm the phase of the catalysts, after growth. (Figure 2(c)). The chemical stoichiometry, as recorded from the EDX spectrum. of the catalyst tip agrees well with the composition of the $FeGe_2$ phase of iron germanide, with 35.0 at.% Fe and 65.0 at.% Ge in the seed particle.

Vapour-liquid-solid (VLS) growth of the Ge nanowires is not possible at our growth temperature of 440 ºC. Considering the Fe-Ge binary phase diagram, the lowest Fe-Ge eutectic temperature of 850 °C is much higher than the nanowire growth temperature. In the three-phase VSS growth paradigm, Ge growth species saturates Fe_2O_3 growth seeds to form the favoured thermodynamic phase, according to the “first phase rule”. The phase of the final germanide compound, which under our conditions is the $FeGe_2$ alloy, depend on the thermodynamic condition under the experimental constrains used. In our typical VSS-type

growth scenario, thermal decomposition of the Ge precursor (in our case DPG) on the surface of the growth catalyst yield to reactive Ge. This Ge adatoms diffuses into the bulk of the starting catalyst material (Fe_2O_3), forming stable germanide compounds ($FeGe_2$), which act as the active catalyst for nanowire growth. This phase transformation cannot be identified *in-situ* but this $FeGe_2$ phase is observed at the nanowire tip (Figure 2 (b)). The lattice mismatch between the stainless-steel and the in-situ formed $FeGe_2$ enables the generation of individual germanide islands which catalyses the Ge nanowire growth. These individual islands can subsequently form a polycrystalline $FeGe_2$ catalytic layer, analogous to observations of Ge nanowires grown from Cu foils.[23] A relatively short growth time (20 min) for Ge nanowires growth on the stainless-steel foils yielded short nanowires (< 1 μm) with spherical tips and unreacted rough granular catalytic film under the grown nanowires (SEM images in Figure S3 in the Supporting Information). Appearance of large amounts of catalytic seed at the nanowire tip (Figure S3) further confirms the participation of a three-phase VSS-type growth paradigm. The rough polycrystalline film with nano-dimensional grains (constituted of Fe and Ge; EDX analysis is Figure S3(c) in the Supporting Information) formed at the surface of the stainless-steel substrates play the role of the catalyst for subsequent Ge nanowire growth. The average diameter (70.2 ± 8.5) of the nano-dimensional particulates is similar to the diameter of the grown nanowires. The grown nanowires and the particulate seeds observed after shot growth time (Figure S3(b) in the Supporting Information)) are thicker than the thickness of the pre-formed oxide layer (assuming it is ≤ 50 nm)[27]. This observation and the appearance of $FeGe_2$ nanoparticles at the tip of the nanowire (Figure 2(b) and (c)) suggest towards a full conversion of the pre-formed Fe_2O_3 layer to $FeGe_2$ during Ge nanowire growth. With the continued flux of the precursor catalytic seed attain supersaturation and the nucleation of the phase pure Ge crystals from the $FeGe_2$ occurs at the triple-phase interface. The sustained growth of one-dimensional Ge single crystals is maintained with the continuous delivery of the Ge source.

Since nanowire growth follows a VSS growth paradigm using germanide forming type-c catalyst, growth is performed far below the lowest eutectic temperatures for a Fe-Ge system, thermodynamic and kinetic factors controlling the formation of the starting germanide compounds are the key in the nucleation of Ge and Ge nanowire growth kinetics.[26] The phase observed at the metallic alloy tip of the nanowires; *i.e*. $FeGe_2$; relates to the kinetic and thermodynamic factors such as the kinetics of the germanide phase formation and the formation of coherent and semi-coherent interfaces to the nanowire surface.[35] Consequently, these kinetic factors are governed by the experimental parameters such as growth temperature, choice of precursor etc.

Cyclic voltammetry (CV) was performed to investigate the lithiation and delithiation of Ge nanowires fabricated on the stainless-steel electrodes. The 1st CV scan, which was acquired at a scan rate of 0.1 mV/s is shown in Figure 3(a). The low intensity peak observed at 0.49 V is due to the lithiation of crystalline Ge (c-Ge).[36] The two strong reduction peaks at ~ 0.19 and 0.09 V are associated with the formation of a-$Li_{15}Ge_4$ and c-$Li_{15}Ge_4$, alloys respectively.[37] From the second cycle onwards, a series of reduction peaks were observed at ~ 0.46, 0.35 and 0.17 V, which are associated with the development of a series of Li−Ge alloys (a-Li_xGe → a-$Li_{15}Ge_4$ → c-$Li_{15}Ge_4$).[38] A sharp oxidation peak can be seen during the initial cathodic sweep at ~ 0.62 V which corresponds to the delithiation of the c-$Li_{15}Ge_4$ phase.[39] This reduction peak became broader and less intense with increased cycling as shown in Figure 3(b). The reason for this broadening will be further during the analysis of differential charge curves.

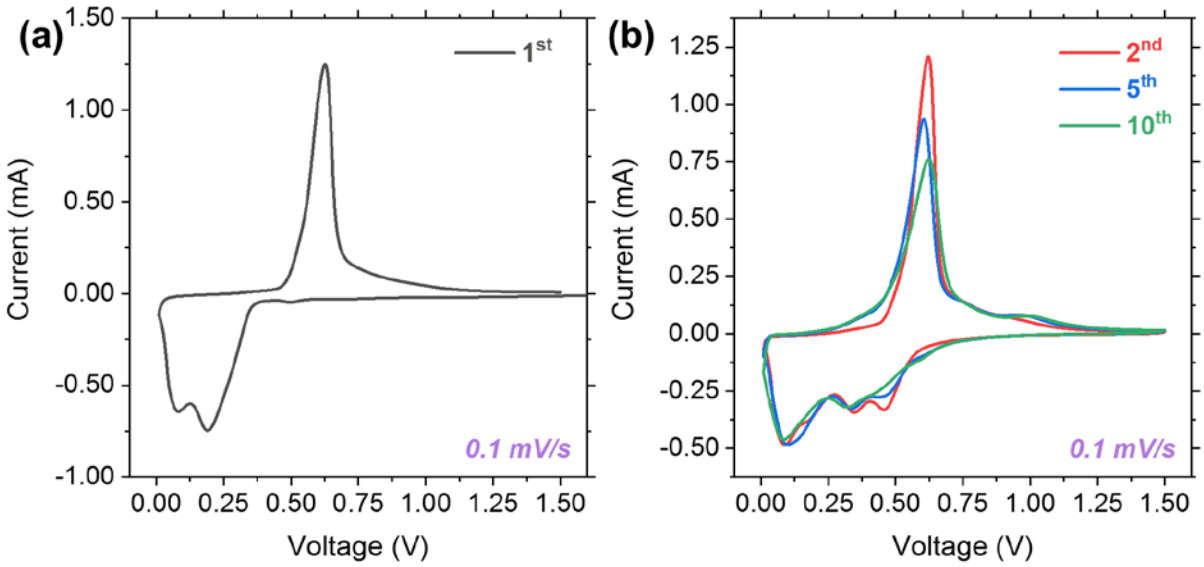

Figure 3. Cyclic voltammograms showing (a) the 1st and (b) the 2nd, 5th and 10th cycles, for Ge nanowires cycled at 0.1 mV/s in a potential window from 1.5 – 0.01 V.

To further evaluate their electrochemical performance, Ge nanowire electrodes were cycled galvanostatically for 250 cycles at a rate of 0.2 C, in a voltage range of 1.50 to 0.01 V (vs Li/Li^+). Voltage profiles ranging from the 1st to the 250th cycle are shown in Figures 4 (a), (b) and (c). During the 1st charge curve (inset of Figure 4a), there was an initial sharp decrease from ~3.20 V down to ~ 0.4 V, which may be attributed to the formation of an solid electrolyte interface (SEI) layer and the lithiation of crystalline Ge.[40] Three reduction plateaux were observed during the initial charge from ~0.35 to 0.26 V, 0.26 to 0.12 V and from 0.12 V to 0.01 V, corresponding to the step-by-step lithiation of the Ge nanowires and the gradual formation of the c-$Li_{15}Ge_4$ phase.[39] The long plateau centred at ~0.5 V during the first discharge is associated with the delithiation of the Ge nanowires.[41] The initial charge and discharge capacities were ~2375 and 1000 mAh/g, respectively, corresponding to an initial Coulombic efficiency (ICE) of ~ 42 %. The large initial charge capacity may be associated with the irreversible lithiation of crystalline Ge as well as formation of an SEI layer on the surface of the Ge NWs. Low ICE is common for Ge electrodes and other alloying mode materials,

including Sn and Si.[42–44] However, from the second cycle onwards the Coulombic efficiency (CE) was > 90%, as indicated by the overlapping voltage profiles in Figure 4a. Three sloping plateaux were observed during the second charge from ~0.7 to 0.4 V, 0.4 to 0.2 V and from 0.2 – 0.01 V, which is agreement with the cyclic voltammograms shown in Figure 3, and corresponds to the formation of a-Li_xGe, a-$Li_{15}Ge_4$, and c-$Li_{15}Ge_4$, respectively. The presence of these plateaux in the charge curves from the 2nd to the 250th cycle, as shown in Figures 4 (a), (b) and (c), indicates a high level of reversibility after the initial lithiation of crystalline Ge during the first charge.

The specific capacities acquired over 250 cycles and the corresponding CE values are shown in Figure 4(d). Ge nanowires, grown directly on stainless-steel, can achieve large capacity values, with a high level of capacity retention. The charge capacity after the 2nd cycle was 1168 mAh/g, which decreased gradually to 1100 mAh/g after the 25th cycle. The CE from the 25th cycle onwards was >98 % and it remained above this value for the rest of the 250 cycles. This is a significantly high level of CE stability for directly grown, non-slurried Ge nanowires. Vinylene carbonate was used as an electrolyte additive to promote stable SEI layer formation and to improve CE. It has previously been demonstrated that VC significantly improves the CE of Ge nanowire based anodes over long term cycling.[37] The specific capacities after the 100th, 200th and 250th charges were 929, 910 and 894 mAh/g respectively. The mean capacity decay per cycle was ~1.1 mAh/g per cycle, which is a further indicator of the impressive stable cycling observed for the Ge nanowires.

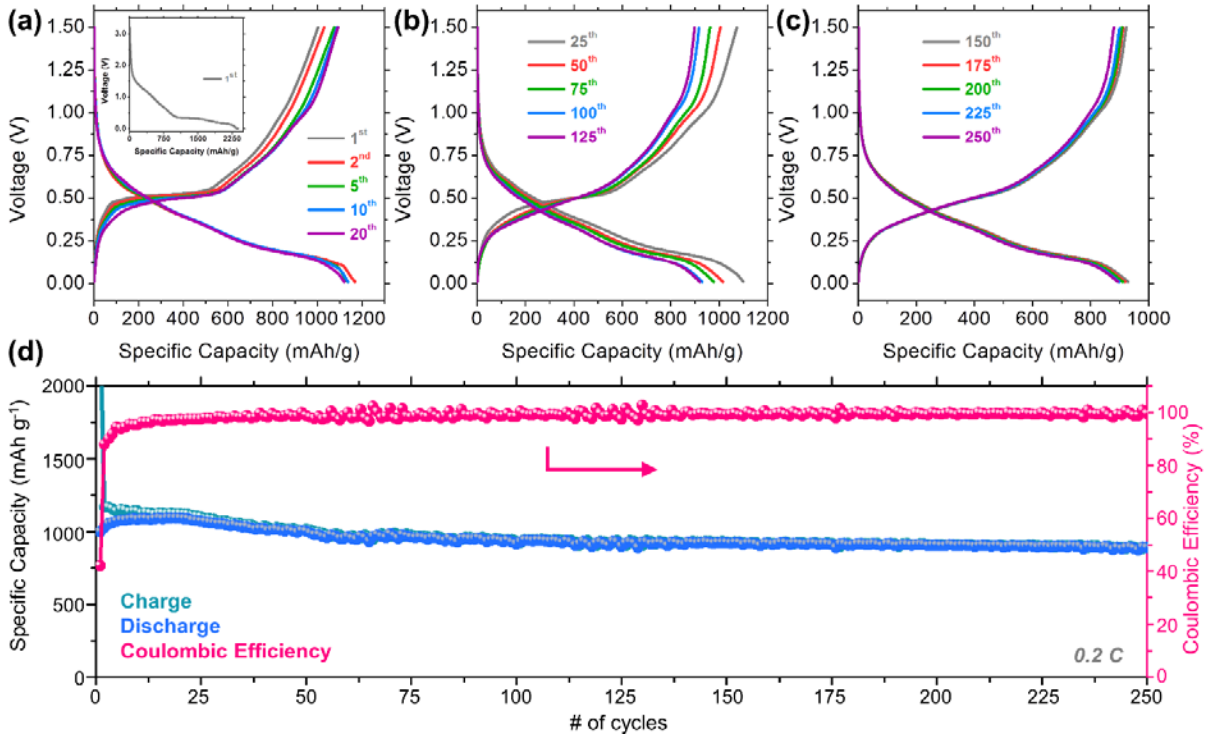

Figure 4. Voltage profiles for (a) the 1st, 2nd, 5th, 10th and 20th cycles, (b) the 25th, 50th, 75th, 100th and 125th cycles and (c) the 150th, 175th, 200th, 225th and 250th cycles for Ge nanowires at 0.2 C in a potential window of 1.50 – 0.01 V (vs Li/Li^+). (d) Specific capacity and Coulombic efficiency values obtained for Ge nanowires.

Differential charge plots (DCPs) were calculated from galvanostatic cycling curves to further investigate the impressive charge storage mechanism of the nanowires. The initial lithiation contained of a series of reduction processes, which are indicated as troughs in the DCP presented in Figure 5(a).[37] The strong, sharp trough centred at 0.35 V is associated with the lithiation of crystalline Ge (c-Ge) and is at its most intense during the first charge. This suggests that the nanowires may not return to a fully delithiated crystalline Ge phase after the initial lithiation process. A similar decrease of the reduction peak after the first cycle was also observed by Mullane *et al*. for Cu catalysed Ge nanowires. [36] The strong trough at 0.19 V is associated with the formation of a-$Li_{15}Ge_4$ and the weaker shoulder at 0.15 V is attributed to the formation of c-$Li_{15}Ge_4$.[37] The wide, asymmetric oxidation peak, observed in the first

cathodic (delithiation) scan from ~0.4 to 0.6 V (Figure 5(b)), can be deconvoluted into two individual peaks, which are centred at 0.48 and 0.52 V. These peaks correspond to the delithiation of the c-$Li_{15}Ge_4$ and a-$Li_{15}Ge_4$ phases. These deconvoluted peaks are shown in Figure S4 in Supporting Information.[45,46] The DCP for the 2nd charge contained three troughs, (Figure 5a). The two broad troughs, centred at ~0.54 and 0.40 V are due to the formation of amorphous Li-Ge alloys, a-Li_xGe and a-$Li_{15}Ge_4$, respectively and the sharp trough at 0.18 V is associated with the formation of c-$Li_{15}Ge_4$.[38,40]

Differential charge contour plots, which were calculated from galvanostatic cycling voltage profiles, from the 2nd to the 250th cycle are shown in Figures 5(c) and (d). The two high intensity regions observed in Figure 5(c) are associated with the reduction peaks for the development of a-$Li_{15}Ge_4$ and c-$Li_{15}Ge_4$ phases, centred at ~0.40 and 0.18 V, respectively. The formation of these phases is a highly reversible process, as the troughs remain present throughout the 250 cycles, as shown in Figure 5c. The consistency of these reduction troughs likely results in the remarkable capacity retention of the nanowires. The differential charge contour plot, calculated from delithiation voltage profiles, is shown in Figure 5(d). The oxidation peak, is attributed to the delithiation of the c-$Li_{15}Ge_4$ and a-$Li_{15}Ge_4$ phases and is still present after 100 cycles. The stacked DCPs (Figure S5) demonstrate that the width of the oxidation peak increases with increased cycling, however it is clear from Figure 4(d) that the discharge capacities do not significantly change, suggesting that the progressive widening of the delithiation peak as the number of cycles increases does not have a significant negative impact on the overall charge stored. The majority of charge stored during lithiation is initially primarily due to the formation of the c-$Li_{15}Ge_4$ phase. With increased cycling the intensity of this reduction trough gradually decreases but the overall charge stored remains stable, suggesting that after the initial cycles, the primary charge storage mechanism switches from the formation of the c-$Li_{15}Ge_4$ phase to the formation of the a-$Li_{15}Ge_4$ phase. This change

would also result in a broadening of the oxidation peak, as observed in Figure 5(d) and Figure S5. The same trend has previously been reported for for GeO_2 inverse opal structured anodes, whereby after initial cycling, more charge was stored due to the formation of the a-$Li_{15}Ge_4$ phase rather than the c-$Li_{15}Ge_4$ phase.[39]

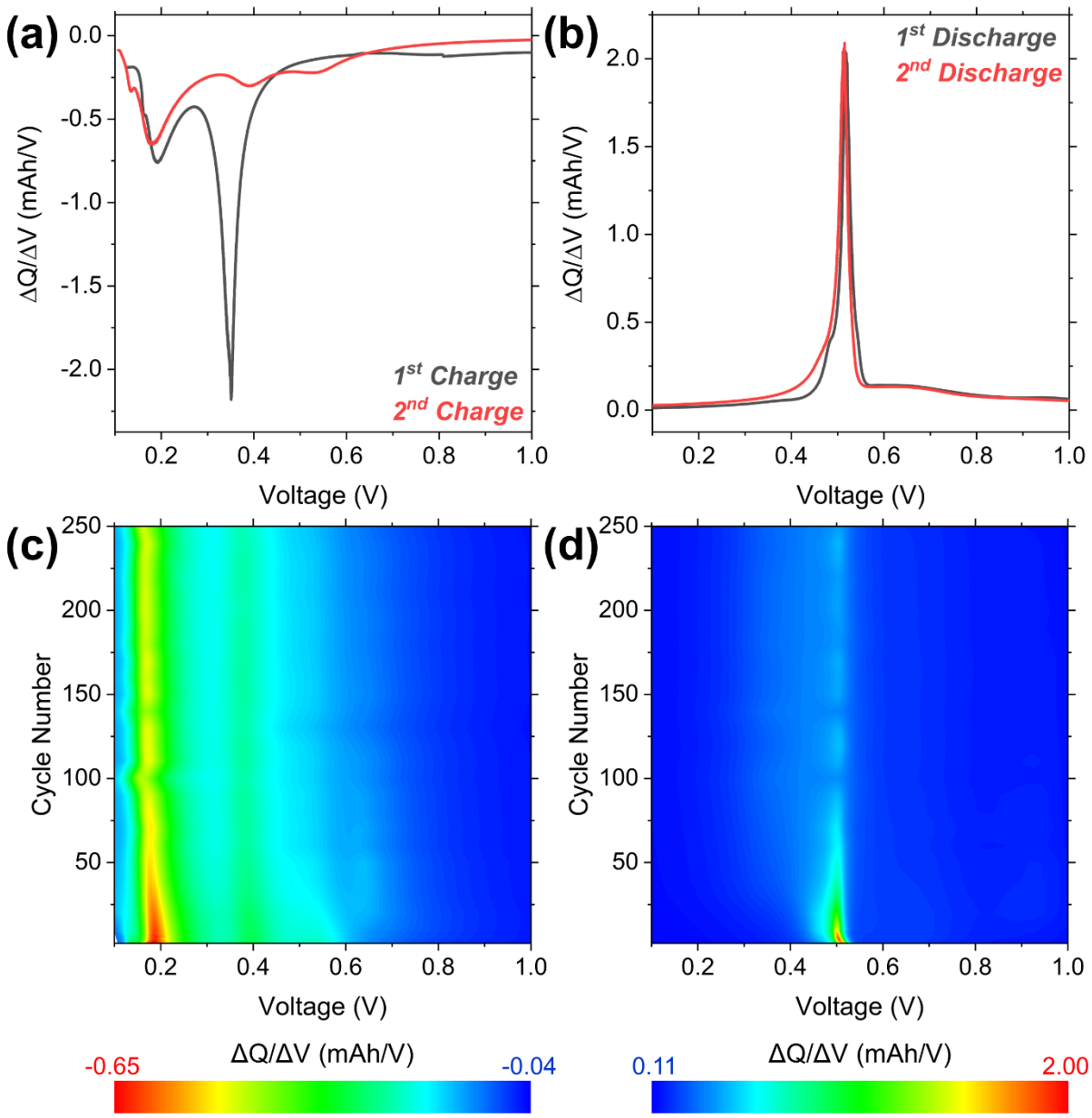

Figure 5. (a) Differential charge plots (DCPs) calculated from the 1st and 2nd galvanostatic charges at 0.2 C. (b) DCPs calculated from the 1st and 2nd galvanostatic discharges at 0.2 C. (c) Contour DCP calculated from differential charge curves from the 2nd to the 250th charge.

(d) Contour DCP calculated from differential discharge curves from the 2nd to the 250th discharge.

The specific capacities that our Ge nanowire anodes delivered are comparable to and in some cases greater than previously reported values for Ge based anode materials.[37,43,47–51] Ge nanowires are typically grown on a substrate via a CVD process involving a catalytic seed.[52–54] Our Ge nanowires, which are directly grown on stainless-steel current collecting substrates, do not require an initial processing step to decorate the substrate with metal nanoparticle seeds. Some commonly used metal seeds, such as Au, form irreversible alloys with Li during cycling and result in lower capacity values due to the dead-weight of these electrochemically inactive seeds.[21] Direct growth on stainless steel current collectors also negates the requirement of nanowire transfer process from the growth substrate to current collector. In this regard, the direct growth may prevent after-growth oxidation of the stainless steel-nanowire contact, ensuring oxide free barriers at the nanowire anode-current collector interface. Additionally, we did not observe any voltage plateau associated with the Li-ion intercalation with Fe_2O_3 or reduction of Fe ions, in the DCP charge curve (Figure 5(a)).[55] This indicates that the pre-formed catalytic Fe_2O_3 layer on the stainless steel current collector is not present at the nanowire-stainless steel interface in the Ge nanowire sample, *i.e.* fully consumed during Ge nanowire growth. Compressed nanowires in the split coin cell also ensures that the contact point of nanowire to the stainless steel substrate is maintained, resulting in good electrochemical performance. After 250 cycles, there was a significant deformation and restructuring of the nanowire morphology and an amorphisation of the Ge nanowires (STEM image in Figure S6 in Supporting Information). The conversion of individual crystalline nanowires to an amorphous mesh was previously reported for Ge nanowires even after 100 cycles.[37]

Additionally, another distinction between our samples and typical Ge anodes is the lack of binder and conductive additive, which were rendered redundant due to our novel direct growth method. The preparation of composite anodes with carbon-based materials may lead to artificially inflated capacity values as carbon stores charge but the mass of conductive additives is typically not considered when calculating the specific capacity of such electrodes; graphite and its various forms are lithiated within the voltage range that Ge is typically cycled in (1.5 – 0.01 V, vs Li/Li^+). Graphite and graphene nanosheets are known to achieve capacities of 320 and 540 mAh/g, respectively, when cycled against Li metal[56], demonstrating that the mass of conductive additives should be taken into account when determining the specific capacities for anode slurry electrodes. Considering this, the specific capacities, obtained with the Ge nanowires in this work are even more impressive as we achieved a state-of-the-art response, without the need to include binders and conductive additives.

Conclusions

In summary, successful bottom-up growth of Ge nanowires was achieved on oxidised stainless-steel without any additional metal nanoparticle seeds. Stainless-steel substrates were heated in air to form Fe_2O_3 surface films which can be converted to $FeGe_2$ seeds for Ge nanowire growth. This unique growth method eliminates the need to deposit metal nanoparticles such as Au or Sn on substrates prior to CVD synthesis of nanowires. This elegant workaround simplifies Ge nanowire growth by removing a complex and expensive processing step. We demonstrate that the yield of Ge nanowires is significantly increased when they are grown on oxidised stainless steel substrates compared to untreated, as-received stainless-steel. The electrochemical performance of the nanowires was determined via a correlation of results from cyclic voltammetry and galvanostatic cycling. The substrate grown Ge nanowires

exhibited impressive capacity retention, when cycled at 0.2 C. The average capacity decay per cycle was ~1.1 mAh/g per cycle, which demonstrates the exceptionally stable cycling observed for the nanowires. Significantly large capacity values with a high level of capacity retention over 250 cycles can be obtained from Ge nanowires grown directly on stainless-steel. The analysis ofdifferential charge plots demonstrated that the alloying of the Ge nanowires with Li is a highly reversible process, as the corresponding reduction and oxidation peaks were consistently present throughout 250 cycles. We demonstrate that it is not necessary to prepare metallic seeds via complex processing procedures to obtain Ge nanowires, which are capable of delivering high specific capacities, representing a significant advancement for nanostructured alloying mode anode materials. The exceptional performance of our nanowires is likely due to their direct growth on the current collecting substrate, which provides a large surface area of active material in direct contact with the electrolyte and excellent anchoring to the current collector. To our knowledge, the specific capacities achieved with our substrate grown Ge nanowires are among the highest values ever reported for Ge nanowires, therefore demonstrating the advantages of directly growing Ge nanowires, or other nanowire anode materials, on an electrically conductive substrates.

Supporting Information

Supporting Information content experimental description and detail on characterization techniques, XPS analysis and SEM of oxidised stainless steel, Raman spectroscopy, additional STEM and SEM images of nanowires and post-cycled nanowires, DCP for different discharge curves.

Author Contribution

D.M. and S.B. contributed equally in writing this manuscript.

Acknowledgements

This research was funded by Science Foundation Ireland (Grant No: 14/IA/2513 and 14/IA/2581).

Conflict of Interest

The authors declare no competing financial interest.

References:

(1) McNulty, D.; Noel Buckley, D.; O'Dwyer, C. NaV2O5 from Sodium Ion-Exchanged Vanadium Oxide Nanotubes and Its Efficient Reversible Lithiation as a Li-Ion Anode Material. *ACS Appl. Energy Mater.* **2019**, *2* (1), 822–832. https://doi.org/10.1021/acsaem.8b01895.

(2) McNulty, D.; Carroll, E.; O'Dwyer, C. Rutile TiO2 Inverse Opal Anodes for Li-Ion Batteries with Long Cycle Life, High-Rate Capability, and High Structural Stability. *Adv. Energy Mater.* **2017**, *7* (12), 1602291. https://doi.org/10.1002/aenm.201602291.

(3) Geaney, H.; McNulty, D.; O'Connell, J.; Holmes, J. D.; O'Dwyer, C. Assessing Charge Contribution from Thermally Treated Ni Foam as Current Collectors for Li-Ion Batteries. *J. Electrochem. Soc.* **2016**, *163* (8), A1805–A1811. https://doi.org/10.1149/2.0071609jes.

(4) Stokes, K.; Geaney, H.; Sheehan, M.; Borsa, D.; Ryan, K. M. Copper Silicide Nanowires as Hosts for Amorphous Si Deposition as a Route to Produce High Capacity Lithium-Ion Battery Anodes. *Nano Lett.* **2019**, *19* (12), 8829–8835. https://doi.org/10.1021/acs.nanolett.9b03664.

(5) Qi, W.; Shapter, J. G.; Wu, Q.; Yin, T.; Gao, G.; Cui, D. Nanostructured Anode Materials for Lithium-Ion Batteries: Principle, Recent Progress and Future Perspectives. *J. Mater. Chem. A* **2017**, *5* (37), 19521–19540. https://doi.org/10.1039/c7ta05283a.

(6) Tian, H.; Xin, F.; Wang, X.; He, W.; Han, W. High Capacity Group-IV Elements (Si, Ge, Sn) Based Anodes for Lithium-Ion Batteries. *J. Mater.* **2015**, *1* (3), 153–169. https://doi.org/10.1016/j.jmat.2015.06.002.

(7) Aghazadeh Meshgi, M.; Biswas, S.; McNulty, D.; O'Dwyer, C.; Alessio Verni, G.; O'Connell, J.; Davitt, F.; Letofsky-Papst, I.; Poelt, P.; Holmes, J. D.; Marschner, C. Rapid, Low-Temperature Synthesis of Germanium Nanowires from Oligosilylgermane

Precursors. *Chem. Mater.* **2017**, *29* (10), 4351–4360. https://doi.org/10.1021/acs.chemmater.7b00714.

(8) Bogart, T. D.; Oka, D.; Lu, X.; Gu, M.; Wang, C.; Korgel, B. A. Lithium Ion Battery Peformance of Silicon Nanowires with Carbon Skin. *ACS Nano* **2014**, *8* (1), 915–922. https://doi.org/10.1021/nn405710w.

(9) Wang, D.; Chang, Y. L.; Wang, Q.; Cao, J.; Farmer, D. B.; Gordon, R. G.; Dai, H. Surface Chemistry and Electrical Properties of Germanium Nanowires. *J. Am. Chem. Soc.* **2004**, *126* (37), 11602–11611. https://doi.org/10.1021/ja047435x.

(10) Graetz, J.; Ahn, C. C.; Yazami, R.; Fultz, B. Nanocrystalline and Thin Film Germanium Electrodes with High Lithium Capacity and High Rate Capabilities. *J. Electrochem. Soc.* **2004**, *151* (5), A698. https://doi.org/10.1149/1.1697412.

(11) Lee, H.; Kim, M. G.; Choi, C. H.; Sun, Y. K.; Yoon, C. S.; Cho, J. Surface-Stabilized Amorphous Germanium Nanoparticles for Lithium-Storage Material. *J. Phys. Chem. B* **2005**, *109* (44), 20719–20723. https://doi.org/10.1021/jp052620y.

(12) Lee, G. H.; Kwon, S. J.; Park, K. S.; Kang, J. G.; Park, J. G.; Lee, S.; Kim, J. C.; Shim, H. W.; Kim, D. W. Germanium Microflower-on-Nanostem as a High-Performance Lithium Ion Battery Electrode. *Sci. Rep.* **2014**, *4* (1), 6883. https://doi.org/10.1038/srep06883.

(13) Park, M. H.; Cho, Y.; Kim, K.; Kim, J.; Liu, M.; Cho, J. Germanium Nanotubes Prepared by Using the Kirkendall Effect as Anodes for High-Rate Lithium Batteries. *Angew. Chemie - Int. Ed.* **2011**, *50* (41), 9647–9650. https://doi.org/10.1002/anie.201103062.

(14) Doherty, J.; Biswas, S.; McNulty, D.; Downing, C.; Raha, S.; O'Regan, C.; Singha, A.; O'Dwyer, C.; Holmes, J. D. One-Step Fabrication of GeSn Branched Nanowires. *Chem. Mater.* **2019**, *31*, 4016–4024. https://doi.org/10.1021/acs.chemmater.9b00475.

(15) Biswas, S.; O'Regan, C.; Petkov, N.; Morris, M. A.; Holmes, J. D. Manipulating the Growth Kinetics of Vapor-Liquid-Solid Propagated Ge Nanowires. *Nano Lett.* **2013**, *13* (9), 4044–4052. https://doi.org/10.1021/nl401250x.

(16) Lu, X.; Harris, J. T.; Villarreal, J. E.; Chockla, A. M.; Korgel, B. A. Enhanced Nickel-Seeded Synthesis of Germanium Nanowires. *Chem. Mater.* **2013**, *25* (10), 2172–2177. https://doi.org/10.1021/cm401047w.

(17) Mullane, E.; Kennedy, T.; Geaney, H.; Dickinson, C.; Ryan, K. M. Synthesis of Tin Catalyzed Silicon and Germanium Nanowires in a Solvent-Vapor System and Optimization of the Seed/Nanowire Interface for Dual Lithium Cycling. *Chem. Mater.* **2013**, *25* (9), 1816–1822. https://doi.org/10.1021/cm400367v.

(18) Flynn, G.; Palaniappan, K.; Sheehan, M.; Kennedy, T.; Ryan, K. M. Solution Synthesis of Lead Seeded Germanium Nanowires and Branched Nanowire Networks and Their Application as Li-Ion Battery Anodes. *Nanotechnology* **2017**, *28* (25). https://doi.org/10.1088/1361-6528/aa72c7.

(19) Doherty, J.; McNulty, D.; Biswas, S.; Moore, K.; Conroy, M.; Bangert, U.; O'Dwyer, C.; Holmes, J. D. Germanium Tin Alloy Nanowires as Anode Materials for High Performance Li-Ion Batteries. *Nanotechnology* **2020**, *31* (16). https://doi.org/10.1088/1361-6528/ab6678.

(20) Geaney, H.; Bree, G.; Stokes, K.; Collins, G. A.; Aminu, I. S.; Kennedy, T.; Ryan, K.

M. Enhancing the Performance of Germanium Nanowire Anodes for Li-Ion Batteries by Direct Growth on Textured Copper. *Chem. Commun.* **2019**, *55* (54), 7780–7783. https://doi.org/10.1039/c9cc03579f.

(21) Chockla, A. M.; Bogart, T. D.; Hessel, C. M.; Klavetter, K. C.; Mullins, C. B.; Korgel, B. A. Influences of Gold, Binder and Electrolyte on Silicon Nanowire Performance in Li-Ion Batteries. *J. Phys. Chem. C* **2012**, *116* (34), 18079–18086. https://doi.org/10.1021/jp305371v.

(22) Richards, B. T.; Gaskey, B.; Levin, B. D. A.; Whitham, K.; Muller, D.; Hanrath, T. Direct Growth of Germanium and Silicon Nanowires on Metal Films. *J. Mater. Chem. C* **2014**, *2* (10), 1869–1878. https://doi.org/10.1039/c3tc31666a.

(23) Geaney, H.; Dickinson, C.; Barrett, C. A.; Ryan, K. M. High Density Germanium Nanowire Growth Directly from Copper Foil by Self-Induced Solid Seeding. *Chem. Mater.* **2011**, *23* (21), 4838–4843. https://doi.org/10.1021/cm202276m.

(24) Cui, L. F.; Ruffo, R.; Chan, C. K.; Peng, H.; Cui, Y. Crystalline-Amorphous Core-Shell Silicon Nanowires for High Capacity and High Current Battery Electrodes. *Nano Lett.* **2009**, *9* (1), 491–495. https://doi.org/10.1021/nl8036323.

(25) Mathur, S.; Shen, H.; Sivakov, V.; Werner, U. Germanium Nanowires and Core-Shell Nanostructures by Chemical Vapor Deposition of [Ge(C5H5)2]. *Chem. Mater.* **2004**, *16* (12), 2449–2456. https://doi.org/10.1021/cm031175l.

(26) Biswas, S.; Doherty, J.; Majumdar, D.; Ghoshal, T.; Rahme, K.; Conroy, M.; Singha, A.; Morris, M. A.; Holmes, J. D. Diameter-Controlled Germanium Nanowires with Lamellar Twinning and Polytypes. *Chem. Mater.* **2015**, *27* (9), 3408–3416. https://doi.org/10.1021/acs.chemmater.5b00697.

(27) Vesel, A.; Mozetic, M.; Drenik, A.; Hauptman, N.; Balat-Pichelin, M. High Temperature Oxidation of Stainless Steel AISI316L in Air Plasma. *Appl. Surf. Sci.* **2008**. https://doi.org/10.1016/j.apsusc.2008.06.017.

(28) Olsen, A.; Sale, F. R. Growth Kinetics and Morphologies of Iron Silicide Layers. *J. Mater. Sci.* **1978**, *13* (10), 2157–2163. https://doi.org/10.1007/BF00541669.

(29) Wei, L. Y. Diffusion of Silver, Cobalt and Iron in Germanium*. *J. Phys. Chem. Solids* **1961**, *18* (2–3), 162–174. https://doi.org/10.1016/0022-3697(61)90159-7.

(30) Barth, S.; Koleśnik, M. M.; Donegan, K.; Krstić, V.; Holmes, J. D. Diameter-Controlled Solid-Phase Seeding of Germanium Nanowires: Structural Characterization and Electrical Transport Properties. *Chem. Mater.* **2011**, *23* (14), 3335–3340. https://doi.org/10.1021/cm200646e.

(31) Lee, D. C.; Mikulec, F. V.; Korgel, B. A. Carbon Nanotube Synthesis in Supercritical Toluene. *J. Am. Chem. Soc.* **2004**, *126* (15), 4951–4957. https://doi.org/10.1021/ja031522s.

(32) McNulty, D.; Geaney, H.; Carroll, E.; Garvey, S.; Lonergan, A.; O'Dwyer, C. The Effect of Particle Size, Morphology and C-Rates on 3D Structured Co3O4 Inverse Opal Conversion Mode Anode Materials. *Mater. Res. Express* **2017**, *4* (2), 25011. https://doi.org/10.1088/2053-1591/aa5a26.

(33) McNulty, D.; Geaney, H.; Armstrong, E.; O'Dwyer, C. High Performance Inverse Opal Li-Ion Battery with Paired Intercalation and Conversion Mode Electrodes. *J. Mater.*

Chem. A **2016**, *4* (12), 4448–4456. https://doi.org/10.1039/c6ta00338a.

(34) Majumdar, D.; Biswas, S.; Ghoshal, T.; Holmes, J. D.; Singha, A. Probing Thermal Flux in Twinned Ge Nanowires through Raman Spectroscopy. *ACS Appl. Mater. Interfaces* **2015**, *7* (44), 24679–24685. https://doi.org/10.1021/acsami.5b07025.

(35) Lensch-Falk, J. L.; Hemesath, E. R.; Perea, D. E.; Lauhon, L. J. Alternative Catalysts for VSS Growth of Silicon and Germanium Nanowires. *J. Mater. Chem.* **2009**, *19* (7), 849–857. https://doi.org/10.1039/b817391e.

(36) Mullane, E.; Kennedy, T.; Geaney, H.; Ryan, K. M. A Rapid, Solvent-Free Protocol for the Synthesis of Germanium Nanowire Lithium-Ion Anodes with a Long Cycle Life and High Rate Capability. *ACS Appl. Mater. Interfaces* **2014**, *6* (21), 18800–18807. https://doi.org/10.1021/am5045168.

(37) Kennedy, T.; Mullane, E.; Geaney, H.; Osiak, M.; O'Dwyer, C.; Ryan, K. M. High-Performance Germanium Nanowire-Based Lithium-Ion Battery Anodes Extending over 1000 Cycles through in Situ Formation of a Continuous Porous Network. *Nano Lett.* **2014**, *14* (2), 716–723. https://doi.org/10.1021/nl403979s.

(38) Baggetto, L.; Notten, P. H. L. Lithium-Ion (De)Insertion Reaction of Germanium Thin-Film Electrodes: An Electrochemical and In Situ XRD Study. *J. Electrochem. Soc.* **2009**, *156* (3), A169. https://doi.org/10.1149/1.3055984.

(39) McNulty, D.; Geaney, H.; Buckley, D.; O'Dwyer, C. High Capacity Binder-Free Nanocrystalline GeO2 Inverse Opal Anodes for Li-Ion Batteries with Long Cycle Life and Stable Cell Voltage. *Nano Energy* **2018**, *43*, 11–21. https://doi.org/10.1016/j.nanoen.2017.11.007.

(40) Liu, X. H.; Huang, S.; Picraux, S. T.; Li, J.; Zhu, T.; Huang, J. Y. Reversible Nanopore Formation in Ge Nanowires during Lithiation- Delithiation Cycling: An in Situ Transmission Electron Microscopy Study. *Nano Lett.* **2011**, *11* (9), 3991–3997. https://doi.org/10.1021/nl2024118.

(41) Dileo, R. A.; Frisco, S.; Ganter, M. J.; Rogers, R. E.; Raffaelle, R. P.; Landi, B. J. Hybrid Germanium Nanoparticle-Single-Wall Carbon Nanotube Free-Standing Anodes for Lithium Ion Batteries. *J. Phys. Chem. C* **2011**, *115* (45), 22609–22614. https://doi.org/10.1021/jp205992w.

(42) Kim, G. T.; Kennedy, T.; Brandon, M.; Geaney, H.; Ryan, K. M.; Passerini, S.; Appetecchi, G. B. Behavior of Germanium and Silicon Nanowire Anodes with Ionic Liquid Electrolytes. *ACS Nano* **2017**, *11* (6), 5933–5943. https://doi.org/10.1021/acsnano.7b01705.

(43) Chockla, A. M.; Klavetter, K. C.; Mullins, C. B.; Korgel, B. A. Solution-Grown Germanium Nanowire Anodes for Lithium-Ion Batteries. *ACS Appl. Mater. Interfaces* **2012**, *4* (9), 4658–4664. https://doi.org/10.1021/am3010253.

(44) Lu, B.; Hu, R.; Liu, J.; Liu, J.; Wang, H.; Zhu, M. Improved Coulombic Efficiency and Cycleability of SnO2-Cu-Graphite Composite Anode with Dual Scale Embedding Structure. *RSC Adv.* **2016**, *6* (16), 13384–13391. https://doi.org/10.1039/c5ra23988e.

(45) Yoon, S.; Park, C. M.; Sohn, H. J. Electrochemical Characterizations of Germanium and Carbon-Coated Germanium Composite Anode for Lithium-Ion Batteries. *Electrochem. Solid-State Lett.* **2008**, *11* (4), A42. https://doi.org/10.1149/1.2836481.

(46) Lim, L. Y.; Fan, S.; Hng, H. H.; Toney, M. F. Operando X-Ray Studies of Crystalline Ge Anodes with Different Conductive Additives. *J. Phys. Chem. C* **2015**, *119* (40), 22772–22777. https://doi.org/10.1021/acs.jpcc.5b05857.

(47) Qiang, T.; Fang, J.; Song, Y.; Ma, Q.; Ye, M.; Fang, Z.; Geng, B. Ge@C Core-Shell Nanostructures for Improved Anode Rate Performance in Lithium-Ion Batteries. *RSC Adv.* **2015**, *5* (22), 17070–17075. https://doi.org/10.1039/c4ra16242k.

(48) Guo, W.; Mei, L.; Feng, Q.; Ma, J. Facile Synthesis of Ge/C Nanocomposite as Superior Battery Anode Material. *Mater. Chem. Phys.* **2015**, *168*, 6–9. https://doi.org/10.1016/j.matchemphys.2015.11.016.

(49) Choe, H. S.; Kim, S. J.; Kim, M. C.; Kim, D. M.; Lee, G. H.; Han, S. B.; Kwak, D. H.; Park, K. W. Synthesis of Ge/C Composites as Anodes Using Glucose as a Reductant and Carbon Source for Lithium-Ion Batteries. *RSC Adv.* **2016**, *6* (77), 72926–72932. https://doi.org/10.1039/c6ra14323g.

(50) Li, W.; Yang, Z.; Cheng, J.; Zhong, X.; Gu, L.; Yu, Y. Germanium Nanoparticles Encapsulated in Flexible Carbon Nanofibers as Self-Supported Electrodes for High Performance Lithium-Ion Batteries. *Nanoscale* **2014**, *6* (9), 4532–4537. https://doi.org/10.1039/c4nr00140k.

(51) Lee, G. H.; Shim, H. W.; Kim, D. W. Superior Long-Life and High-Rate Ge Nanoarrays Anchored on Cu/C Nanowire Frameworks for Li-Ion Battery Electrodes. *Nano Energy* **2015**, *13*, 218–225. https://doi.org/10.1016/j.nanoen.2015.02.023.

(52) O'Regan, C.; Biswas, S.; O'Kelly, C.; Jung, S. J.; Boland, J. J.; Petkov, N.; Holmes, J. D. Engineering the Growth of Germanium Nanowires by Tuning the Supersaturation of Au/Ge Binary Alloy Catalysts. *Chem. Mater.* **2013**. https://doi.org/10.1021/cm401281y.

(53) Wang, D.; Dai, H. Low-Temperature Synthesis of Single-Crystal Germanium Nanowires by Chemical Vapor Deposition. *Angew. Chemie - Int. Ed.* **2002**, *41* (24), 4783–4786. https://doi.org/10.1002/anie.200290047.

(54) Biswas, S.; Singha, A.; Morris, M. A.; Holmes, J. D. Inherent Control of Growth, Morphology, and Defect Formation in Germanium Nanowires. *Nano Lett.* **2012**, *12* (11), 5654–5663. https://doi.org/10.1021/nl302800u.

(55) Reddy, M. V.; Yu, T.; Sow, C. H.; Shen, Z. X.; Lim, C. T.; Rao, G. V. S.; Chowdari, B. V. R. α-Fe2O3 Nanoflakes as an Anode Material for Li-Ion Batteries. *Adv. Funct. Mater.* **2007**, *17* (15), 2792–2799. https://doi.org/10.1002/adfm.200601186.

(56) Yoo, E. J.; Kim, J.; Hosono, E.; Zhou, H. S.; Kudo, T.; Honma, I. Large Reversible Li Storage of Graphene Nanosheet Families for Use in Rechargeable Lithium Ion Batteries. *Nano Lett.* **2008**, *8* (8), 2277–2282. https://doi.org/10.1021/nl800957b.

For Table of Contents Only